JACS
JOURNAL OF THE AMERICAN CHEMICAL SOCIETY

ARTICLE

pubs.acs.org/JACS

Dually Switchable Heterotetracenes: Addressing the Photophysical Properties and Self-Organization of the P−S System

Yi Ren and Thomas Baumgartner*

Department of Chemistry, University of Calgary, 2500 University Drive NW, Calgary, AB T2N 1N4, Canada

Supporting Information

ABSTRACT: New ladder-type, phosphorus- and sulfur-based heterotetracenes were synthesized, which allowed the engineering of the materials' properties by exploitation of the different reactivities between sulfur and phosphorus. ^{31}P NMR spectroscopy and X-ray crystallographic studies revealed that the different electronic effects of the secondary heteroatom, sulfur, influence not only the conjugation in the heterotetracene core but also the behavior of the phosphorus center. UV−vis and fluorescence spectroscopy showed that the scaffold's band gap is mainly controlled by the electronic nature of sulfur, while the fluorescence quantum yield highly depends on the electronic nature of phosphorus. Cyclic voltammetry indicated that the redox properties of the system could be altered by selective modification of the respective heteroatom (oxidation of sulfur and/or functionalization of trivalent phosphorus). Importantly, oxidation of the phosphorus center results in enhanced reduction features of the heterotetracene system, and oxidation of the sulfur center further enhances the electron acceptor character of the core. Theoretical calculations provided insights on both selectivity of phosphorus chemistry *and* communication between the two heteroatoms (sulfur and phosphorus). Macroscopic self-organization of the heterotetracenes was observed when the tetracene core is functionalized with pendant functional groups. Preliminary results showed that extension of the molecule with an alkyl chain along the long axis of molecules induces the formation of 1D microfibers, which was confirmed by fluorescence microscopy and scanning electron microscopy.

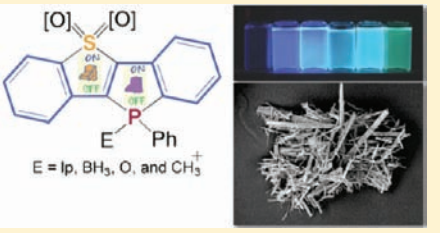

1. INTRODUCTION

Ladder-type π-conjugated molecules exhibit intriguing properties, such as high fluorescence and/or high charge mobility, which have been intensively studied in the context of organic light-emitting diodes (OLEDs), organic field-effect transistors (OFETs), and photovoltaic cells.[1] Although oligoacenes (e.g.: pentacene, tetracene, Chart 1) and their derivatives were the first ladder-type π-conjugated molecules employed in high performance OFETs, their instability toward oxidation sometimes hampers their practical application.[1] The incorporation of main group elements (B, Si, P, and S, Chart 1) into ladder-type π-conjugated molecules provides an intriguing strategy in terms of electronic stabilization and has therefore recently drawn significant attention.[2] Moreover, the different electronic natures of the main group elements can also endow π-conjugated molecules with quite diverse and interesting properties. As the first candidate, sulfur has successfully been introduced in oligoacenes in the form of thiophene units.[3] The high aromaticity of the thiophene ring enhances benzenoid character and, thus, lowers the HOMO energy level with wider HOMO−LUMO band gap, which enhances the photostability and thermal stability of the systems. In addition, weak intermolecular S−S interactions induce preferred face-to-face π-stacking motifs in the solid state, which can increase the electronic coupling between molecules and facilitate charge and energy transport.[4] To further optimize these features, Yamaguchi and others have found that oxidation of sulfur is a very efficient way to enhance the electron-accepting character of thiophene materials.[5,6] However, full oxidation of oligothiophenes, and fused thienoacenes in particular, is still a synthetic challenge and requires rather harsh conditions due to the strong electron-withdrawing effect from a neighboring sulfur dioxide group.[6] Unlike the sulfur atom, boron shows significant electronic coupling with a π-conjugated system, due to the empty p-orbital of the boron center.[7] Differently but similarly efficiently, both silicon and phosphorus interact with a π-conjugated system through hyperconjugation between the σ^*-orbital of exocyclic P/Si−C bonds and the endocyclic π-system of the butadiene moiety that significantly lowers the LUMO energy level.[8,9]

The diverse chemistry and intriguing electronic properties of phosphorus make it a unique member among the main group elements. Réau's and our group were among the first to successfully incorporate phospholes, the P-analogues of thiophenes, into π-conjugated systems in a systematic fashion;[9b,c,10] the phosphorus chemistry (oxidation, methylation, and metalation) allows modifying the photophysical properties of these systems efficiently. Recently, the groups of Yamaguchi, Matano, and our group have demonstrated that the electron-accepting character of heteroacenes can be significantly enhanced via incorporation of phosphorus centers (see, e.g., **IV**, Chart 1).[11] Phosphorus has also been incorporated into π-conjugated systems with other heteroatoms in order to take advantage of the different electronic

Received: June 17, 2010
Published: January 6, 2011

dx.doi.org/10.1021/ja108081b | J. Am. Chem. Soc. 2011, 133, 1328–1340

Chart 1. Tetracenes and Heteroelement-Based Ladder-Type Acenes

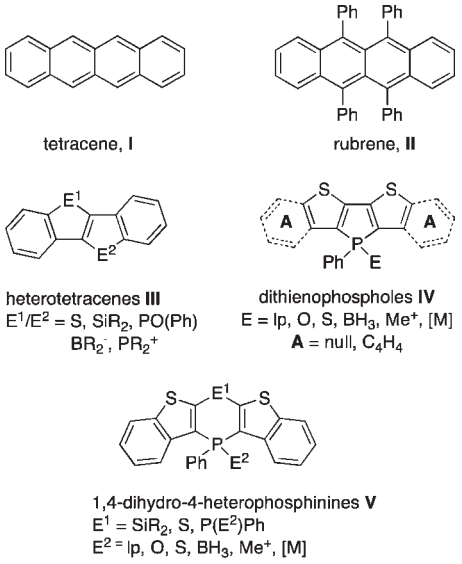

natures of both heteroatoms. Phosphonium- and borate-bridged stilbene systems (**III**, Chart 1), which exhibit very interesting nonlinear optical properties, were reported and systematically studied by Yamaguchi's group.[12] Our recent study on ladder-type phosphinine systems (**V**, Chart 1) has provided insights into the molecular level fine-tuning of the photophysical and electrochemical properties, as well as organization in the solid state caused by geometric and electronic effects of additional heteroatoms (Si, S, and P) in conjunction with phosphorus.[13]

However, the diversity of π-conjugated organophosphorus materials is still limited to date, due to the synthetic challenge when dealing with these compounds; phosphorus behaves fundamentally different from its pnictogen congener nitrogen.[9b] Importantly, the influence of secondary heteroatoms on the phosphorus chemistry and properties of organic materials has not been studied in detail. Herein, we now report the synthesis and structure−property studies of a new phosphorus-based asymmetric heterotetracene system. The photophysical and electrochemical properties of these phosphorus-based heterotetracenes were investigated systematically and correlated with the different electronic natures of the heteroatoms (S and P). The new phosphorus-based heterotetracenes were shown to self-organize into 1D micro-/nanofibers upon functionalization of the core with long alkyl chains along the long axis of the molecular scaffold.

2. RESULTS AND DISCUSSION

2.1. Synthesis. The starting material **1** was obtained via a Suzuki coupling reaction between 2,3-dibromobenzo[*b*]thiophene, which selectively reacts at the 2-position, and 2-bromophenylboronic acid in 73% yield (Scheme 1). Phosphole synthesis following our typical protocol toward dithieno[3,2-*d*:2′,3′-*b*]phospholes[10] gave the asymmetric phosphorus-based heterotetracene **2a** in 70% yield. Compared to the parent dithienophosphole (**IV**, **A** = null, E = lp, Chart 1; δ = −21.5 ppm) and corresponding phosphorus-based heteropentacene (**IV**, **A** = C_4H_4, E = lp, Chart 1; δ = −25.1 ppm), **2a** shows a low-field shifted ^{31}P NMR resonance at δ = −16.5 ppm indicating a relatively higher delocalization of the phosphorus lone pair within the heterotetracene system, which is consistent with theoretical calculations (vide infra) and earlier observations.[10a,11f,13b]

Further functionalization of the phosphorus center (oxidation, methylation, complexation with borane) was carried out following established procedures,[10] providing the products **2b**−**d** in good yields (Scheme 2). The low-field-shifted ^{31}P NMR resonances of δ = 21.3 ppm for **2b**, 26.1 ppm for **2c**, and 14.2 ppm for **2d** clearly supported the formation of the functionalized species. The values are again somewhat low-field-shifted, when compared to the dithienophosphole system (cf. **IV**, **A** = null, E = BH_3, δ = 13.5 ppm; **IV**, **A** = null, E = O, δ = 18.8 ppm; **IV**, **A** = null, E = Me^+, δ = 12.2 ppm; **IV**, **A** = C_4H_4, E = BH_3 16.9 ppm; **IV**, **A** = C_4H_4, E = O, δ = 16.7 ppm; **IV**, **A** = C_4H_4, E = Me^+, δ = 11.4 ppm),[10,11f] likely due to the less pronounced donor character of benzene compared to thiophene. In order to enhance the electron-accepting character of the system, the sulfur center in **2c** was subsequently oxidized with 3 equiv of mCPBA to afford 79% of the sulfur dioxide derivative **3c** with further low-field-shifted ^{31}P NMR resonance (δ = 29.9 ppm). Compared to other ring-fused oligothiophene systems,[5,6] this easy oxidation of the sulfur center in thiophene−phosphole **2c** is probably due to the small electron density change at sulfur upon oxidation of the phosphorus center (vide infra).

The different electronic natures of the sulfur and phosphorus centers drew our attention to the selective reduction of the oxidized phosphole (Scheme 3). Using the same method we have reported before,[10d] phosphole oxide **3c** was transferred into phosphole−borane adduct **3b** ($\delta^{31}P$ = 27.9 ppm) by reacting it with an excess of $BH_3 \cdot SMe_2$. Subsequent treatment with an excess of NEt_3 provided the trivalent phosphole **3a** that shows a typical high-field shift at δ^{31}P = −11.6 ppm that is comparable to the sulfur(II) species **2a** (δ^{31}P = −16.5 ppm). The slight difference can be explained by the electron-withdrawing sulfur dioxide center in **3a**. Notably, the sulfur dioxide center is not reduced during the reduction even with 5 equiv of $BH_3 \cdot SMe_2$, as verified by ^{1}H and ^{31}P NMR spectroscopy. The regenerated trivalent phosphole **3a** could also further be reacted with methyl triflate,[10c,11f] to afford the strongly emissive compound **3d**. It is worth mentioning that the ^{31}P NMR shift difference between phosphonium **3d** (δ = 28.6 ppm) and phosphole oxide **3c** (δ = 29.9 ppm) is smaller than the difference between phosphonium **2d** (δ = 14.2 ppm) and phosphole oxide **2c** (δ = 26.1 ppm), which could be attributed to the electron-withdrawing character of the sulfur dioxide center decreasing the polar character of the exocyclic P=O double bond and therefore shielding the phosphorus center. Compounds **2a**−**d**, **3a**, **3c**, and **3d** were studied by means of Differential Scanning Calorimetry (DSC) and showed good thermal stability without decomposition up to their respective melting points (T_m = 131.6 °C for **2a**, 168.0 °C for **2b**, 164.7 °C for **2c**; 193.4 °C for **2d**; 190.6 °C for **3a**, 208.9 °C for **3c**, and 209.2 °C for **3d**).

2.2. Molecular Structures and Organization in the Solid State. We were able to obtain single crystals of compounds **2c**, **2d**, **3a**, and **3d**. Due to the asymmetric nature of the scaffold, the new heterotetracenes are chiral at the pyramidal phosphorus center. However, both enantiomers are generally found in the unit cells, as determined by X-ray crystallography. Similar to the phosphole-based pentacene systems (**IV**, **A** = C_4H_4, Chart 1) we have reported before,[11f] the five-membered phosphole ring in **2c** shows only a minor deviation from planarity (Figure 1). The sum of the angles around phosphorus is 305.2°, which is typical for phosphole systems.[10] Compared to [1]benzothieno[3,2-*b*]benzothiophene

dx.doi.org/10.1021/ja108081b |*J. Am. Chem. Soc.* 2011, 133, 1328–1340

Scheme 1. Synthesis of the Asymmetric Tetracene 2a

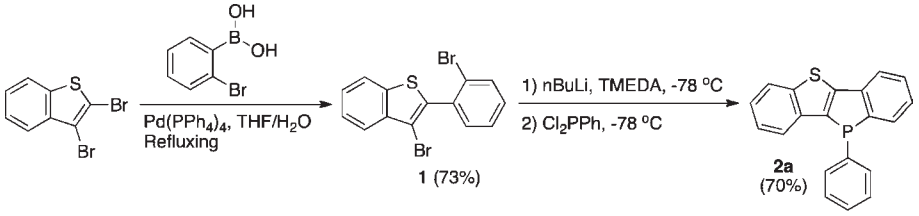

Scheme 2. Functionalization of the Tetracene 2a

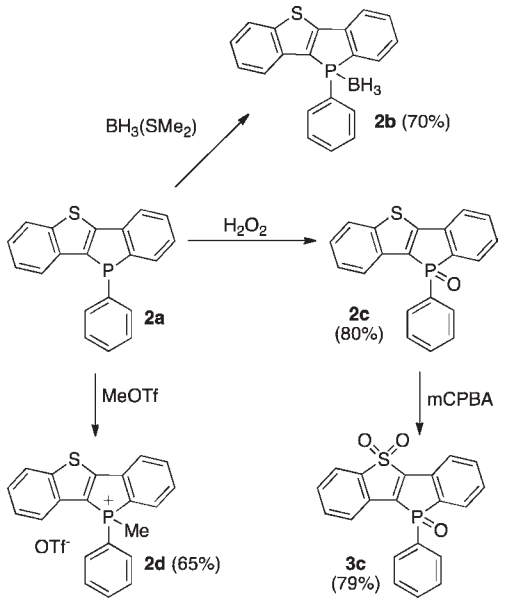

(BTBT, **III**, $E^1 = E^2 = S$, Chart 1),[14a,b] **2c** exhibits similar bond lengths and angles within the thiophene ring, which indicates that the thiophene ring still maintains its aromaticity.

The `benzo' C−C bond lengths of both, the phosphole and thiophene subunits, are identical (C5−C6: 1.409(4) Å and C9−C14: 1.410(3) Å) indicating no significant distortion of the structural parameters of both benzene rings. It should be mentioned in this context that molecular organization in the solid state is also an important feature for both energy and charge transfer in the practical application of molecular materials. BTBT (**III**, $E^1 = E^2 = S$, Chart 1) derivatives with long alkyl chains have been reported to crystallize in a herringbone motif and exhibit CH−π and S−S interactions.[14a,b] With the exocyclic phenyl ring at the phosphorus center, **2c** also organizes in a herringbone arrangement between layers; however, π−π stacking interactions (distance: ca. 3.5 Å) are observed within each layer (see Supporting Information). A similar molecular organization is also observed in the structure of a classical tetracene derivative, rubrene (**II**, Chart 1), with excellent semiconducting properties.[14c,d]

In the phosphonium species **2d**, both the endohedral C−P−C angle (94.2°) and sum of the angles around phosphorus (316.4°) increase due to the phosphorus center approaching tetrahedral geometry (Figure 2). The P−C bond lengths of P1−C8 (1.779(2) Å) and P1−C15 (1.7975(15) Å) are shorter than those in **2c** (P1−C7: 1.792(3) Å, P1−C14: 1.816(2) Å) indicating that the positive phosphonium center polarizes the central C8−C9 `stilbene' double bond more efficiently, which is consistent with the low-field shift of the *ipso*-^{13}C NMR resonance of the thiophene in **2d**. Furthermore, **2d** arranges in dimers in the solid state (see Supporting Information). In addition to a relatively weak π−π interaction (distance: ca. 3.8 Å), a stronger π−π interaction (distance: ca. 3.4 Å) is also observed intradimer, which is probably due to the decreased electron density of the backbone.

As can be seen in the structure of **3a**, oxidation of the sulfur center significantly elongates the sulfur−carbon bonds (S1−C5: 1.774(2) Å, S1−C8: 1.772(2) Å) compared with those in **2c** (cf.: S1−C5: 1.758(3) Å, S1−C8: 1.722(3) Å), which is consistent with the loss of aromaticity upon oxidation of sulfur (Figure 3). The increased endohedral C−S−C angle of 94.2° around sulfur and shortened C7−C8 bond length of 1.344(3) Å further support the significant structural changes in **3a** when compared to **2c**. As for the five-membered phosphole ring, the decreased endohedral C−P−C angle (88.9°) and sum of the angles around phosphorus (297.7°) confirm a more pyramidal geometry. The bonds lengths of the phosphole ring are similar to those of other π-conjugated phospholes[9−11] supporting reduced electronic delocalization within the phosphole ring of **3a**. These changes are consistent with the red-shifted absorption and emission wavelengths of **3a** compared with **2a**, as the conjugation of backbone increases (vide infra). In the solid state, only a very weak intermolecular π−π interaction (distance: ca. 4.0 Å; see Supporting Information) is observed.

Similar to **2d**, the methylation of the phosphorus center increases the sum of angles around phosphorus in **3d** (314.0°; Figure 4). Compared to **3a**, the phosphorus−carbon bonds in **3d** are shortened supporting an increasing communication between the phosphorus center and the π-system, as well as a more rigid backbone. The electron-withdrawing nature of the phosphonium center decreases the electron density of the π-system and, as a result, increases the π−π interactions between molecules in the solid state (distance ca. 3.5 Å; see Supporting Information). In addition, the solid-state organization of **3d** also involves several intermolecular hydrogen bonds between the aromatic ring and the S=O oxygen atoms (distances: 2.47 and 2.51 Å; see Supporting Information).

2.3. Photophysical Properties. Absorption and fluorescence properties of the heterotetracene series **2a**−**d** and **3a**−**d** are summarized in Table 1. Compared to the absorption spectrum of BTBT, **2a** shows similar absorption features in the region λ_{max} = 280−360 nm but a less resolved structure with the maximum at λ_{max} = 317 nm.[14a,15] Functionalization of the phosphorus center modifies the HOMO−LUMO gap of the molecule very efficiently, as evidenced in the red-shifted absorption of the compounds **2a**−**d** (λ_{onset} = 365 nm for **2a**, 376 nm for **2b**, 394 nm for **2c**, and 410 nm for **2d**). The single absorption peaks of **2a** within λ_{max} = 290−370 nm split up into two broad bands in the functionalized phosphorus species **2b**, **2c**, and **2d** indicating that the electronic

dx.doi.org/10.1021/ja108081b |*J. Am. Chem. Soc.* 2011, 133, 1328–1340

Scheme 3. Selective Functionalization of the Phosphorus Center

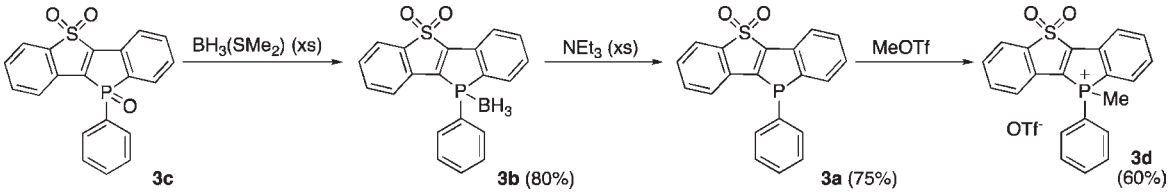

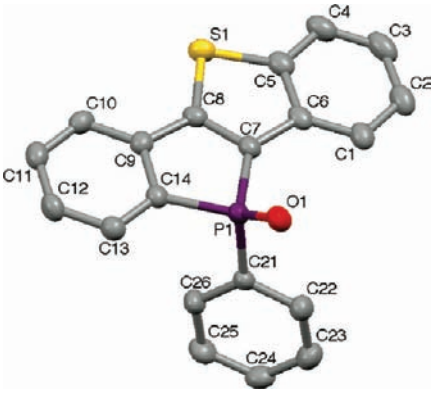

Figure 1. Molecular structure of **2c** in the solid state (50% probability level); hydrogen atoms are omitted for clarity. Selected bond lengths [Å] and angles [deg]: P1−O1: 1.4826(17); P1−C7: 1.792(3); P1−C14: 1.816(2); P2−C21: 1.808(2); C7−C8: 1.365(4); S1−C5: 1.758(3); S1−C8: 1.722(3); C5−C6: 1.409(4); C9−C14: 1.410(3); C5−S1−C8: 90.95(13); C7−P1−C14: 91.74(12); C7−P1−C21: 106.47(12); C14−P1−C21: 106.97(10).

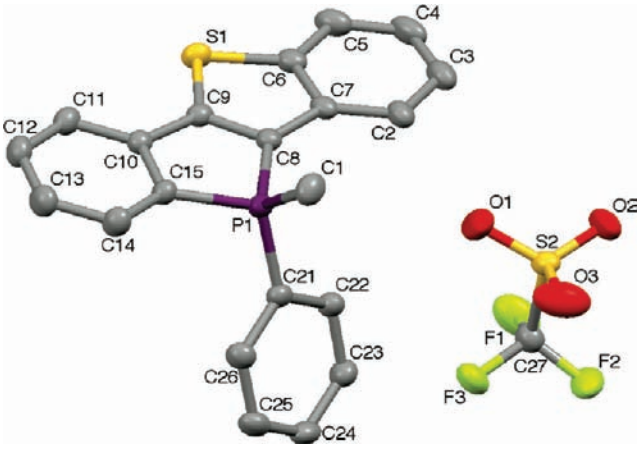

Figure 2. Molecular structure of **2d** in the solid state (50% probability level); hydrogen atoms are omitted for clarity. Selected bond lengths [Å] and angles [deg]: P1−C1: 1.780(2); P1−C8: 1.779(2); P1−C15: 1.7975(19); P1−C21: 1.7954(19); C8−C9: 1.372(3); C6−C7: 1.414(3); C10−C15: 1.408(3); S1−C6: 1.750(2); S1−C9: 1.717(2); C8−P1−C15: 94.20(9); C8−P1−C21: 111.06(9); C15−P1−C21: 111.10(9); C6−S1−C9: 90.60(10).

structure of the system changes significantly (Figure 5, top). Furthermore, as observed in the related trivalent phosphole system by Yamaguchi et al.,[11a] the trivalent phosphole **2a** shows a high molar absorption coefficient of log ε = 4.45, that is comparable with that of BTBT (cf.: log ε = 4.06 at 332 nm, 4.41 at 308 nm, 4.41 at 226 nm, and 4.35 at 258 nm in $CHCl_3$).[15]

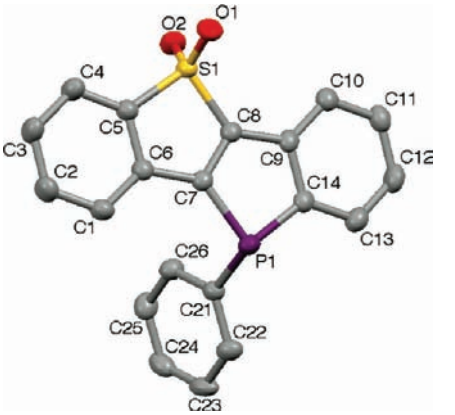

Figure 3. Molecular structure of **3a** in the solid state (50% probability level); hydrogen atoms are omitted for clarity. Selected bond lengths [Å] and angles [deg]: P1−C7: 1.809(2); P1−C14: 1.832(3); P1−C21: 1.826(2); C7−C8: 1.344(3); C5−C6: 1.396(3); C9−C14: 1.414(3); S1−C5: 1.774(2); S1−C8: 1.772(2); S1−O1: 1.4401(18); S1−O2: 1.4435(19); C7−P1−C14: 88.87(11); C7−P1−C21: 103.77(10); C14−P1−C21: 105.8(10); C5−S1−C8: 92.18(11).

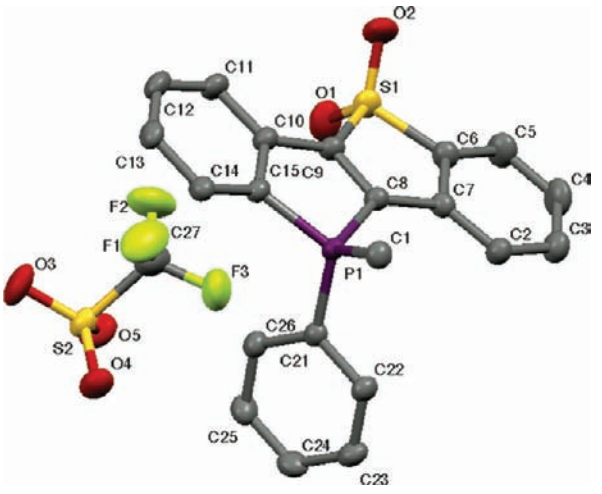

Figure 4. Molecular structure of **3d** in the solid state (50% probability level); hydrogen atoms and one acetone solvent molecule are omitted for clarity. Selected bond lengths [Å] and angles [deg]: P1−C1: 1.773(2); P1−C8: 1.799(2); P1−C15: 1.800(2); P1−C21: 1.785(2); C8−C9: 1.345(3); C6−C7: 1.405(3); C10−C15: 1.408(3); S1−C6: 1.769(2); S1−C9: 1.771(2); S1−O1: 1.435(2); S1−O2: 1.436(2); C8−P1−C15: 92.83(10); C8−P1−C21: 106.65(10); C15−P1−C21: 114.46(10); C6−S1−C9: 92.35(11).

This absorption splitting can be correlated with the elimination of the orbital symmetry in the P-based tetracene cores by functionalization of the phosphorus center, as verified by NMR

dx.doi.org/10.1021/ja108081b |*J. Am. Chem. Soc.* 2011, 133, 1328–1340

Table 1. Photophysical Data for the Heterotetracenes

Compd	λ_{abs} [nm][a]	log ε[c]	E_{op} [eV][d]	λ_{em} [nm]	$\Delta\lambda$ [nm]	ϕ_{PL}[f]	τ [ns][g]	K_r (10^{-7} s^{-1})	K_{nr} (10^{-7} s^{-1})	A [Å][h]
2a	317[b]	4.45	3.40	421[a]	104	0.24	0.3 (70%)	6.7	21.3	3.44
				428[e]			11.2 (30%)			
2b	325[b]	3.43	3.30	400[a]	75	0.38	3.0	12.7	20.7	4.11
				400[e]						
2c	329[b]	3.86	3.15	428[a]	99	0.71	11.3	6.3	2.6	5.48
				434[e]						
2d	340[b]	3.42	3.02	445[a]	105	0.36	14.8	2.4	4.3	4.02
				445[e]						
3a	357[b]	4.21	2.95	453[a]	96	0.14	0.7 (14%)	1.2	7.6	2.75
				471[e]			13.0 (86%)			
3c	386[b]	3.73	2.84	466[a]	80	0.98	12.9	7.6	0.2	8.24
				465[e]						
3d	395[b]	4.33	2.74	483[a]	88	0.99	5.1 (3%)	7.8	0.1	8.96
				485[e]			13.0 (97%)			
4a	343	4.06		428[a]		0.15				
	359[b]	3.94								
	375 (sh)	2.55								
4b	334	4.78		427[a]		0.13				
	359[b]	5.30								
	380 (sh)	3.43								
5a	349	4.27		427[a]		0.29				
	368[b]	4.65								
	381 (sh)	3.75								

[a] Absorption measured in CH_2Cl_2. [b] The lowest energy absorption maxima. [c] ε: Molar absorption coefficient [$L \cdot mol^{-1} \cdot cm^{-1}$]. [d] E_{op}: optical band gap from absorption onset. [e] Solid state. [f] Fluorescence quantum yield was determined by a calibrated integrating sphere system. [g] Fluorescence lifetime. [h] A (Å) = $\ln(K_r/K_{nr}) + 4.6$.

and UV−vis spectroscopy, as well as theoretical calculations (vide infra). The molar absorption coefficients for the P-functionalized derivates, however, are lower than that of **2a** (log ε = 3.43 for **2b**, 3.86 for **2c**, 3.42 for **2d**), which is in line with earlier observations on similar phosphorus-based tetracenes.[11a] As found in other bis-heteroatom-bridged stilbenes, oxidation of the sulfur bathochromically shifts and broadens the absorption spectra (λ_{onset} = 421 nm for **3a**, 437 nm for **3c**, 453 nm for **3d**), due to the electron-withdrawing character of the SO_2 group and the concomitant increase in conjugation within the system (Figure 5, bottom). Importantly, the change of absorption through oxidation of the sulfur ($\Delta\lambda_{onset}$ = 56 nm between **3a** and **2a**) is more significant than functionalization of the phosphorus center ($\Delta\lambda_{onset}$ = 32 nm in **3a**−**d**, 45 nm in **2a**−**d**) suggesting that the band gap of the system is more efficiently controlled by the electronic nature of sulfur (vide infra).

In the nonoxidized sulfur(II) series **2a**−**d**, functionalization of phosphorus does not significantly change the emission wavelengths of the system (λ_{em} = 421 nm for **2a**, 400 nm for **2b**, 428 nm for **2c**, and 445 nm for **2d**) (Figure 6). Similar to the absorption spectra, oxidation of sulfur has a significantly larger effect on the emission wavelengths of the system ($\Delta\lambda_{em}$ = 32 nm between **3a** and **2a**, $\Delta\lambda_{em}$ = 24 nm between **2d** and **2a**), which indicates that the decreasing aromaticity of the thiophene ring enhances the π-conjugation throughout the whole scaffold, essentially converting the system into a heteroatom-bridged *stilbene*, instead of an *oligoacene* (Chart 2).

In CH_2Cl_2, the emission of **2a** is very broad (full width at half-maximum (fwhm) = 95 nm) relative to its congeners (cf.: fwhm = 62 nm for **2b**, 69 nm for **2c**, and 71 nm for **2d**), which further supports the delocalization of the phosphorus lone pair in the excited state (Figure 6).[13b,16] Compared to **2a**, the narrow and blue-shifted emission of **2b** is probably due to both, its weaker electron donor and acceptor character that is consistent with the theoretical calculations. Moreover, the larger Stokes shift of **2a** also implies the existence of structural relaxation in the excited state.[16]

In addition, functionalization of the phosphorus center in the sulfur dioxide series **3**, results in further red-shifted emission features (**3a**: λ_{em} = 453 nm, **3c**: λ_{em} = 466 nm, **3d**: λ_{em} = 483 nm) due to the increasing electron-withdrawing character of the phosphorus center **3a** → **3d** (Figure 6). All compounds in the sulfur dioxide series **3** show similar full widths at half-maximum (fwhm = 82 nm for **3a**, fwhm = 78 nm for **3c**, fwhm = 83 nm for **3d**). In general, the Stokes shift of the phosphole oxide species in both the sulfur(II) series **2a**−**d** and the sulfur dioxide series **3a**−**d** are smaller than those of the nonoxidized species indicating a rigidified system upon oxidation of phosphorus resulting in less rotational freedom for the exocyclic phenyl group due to the partial cationic charge at the pentavalent phosphorus center.

Since oxidation and/or functionalization of the sulfur and phosphorus centers were found to change the electronic nature of the whole π-conjugated scaffold significantly, we decided to also study the solvatochromism of the heterotetracenes (see Supporting Information). However, not all of the compounds do show significant solvatochromism in their in absorption spectra ($\Delta\lambda_{max}$ = 5 nm for **2a**; 2 nm for **2b**; 2 nm for **2c**; 5 nm for **2d**, 8 nm for **3a**; 6 nm for **3c**). In the nonoxidized sulfur(II) series,

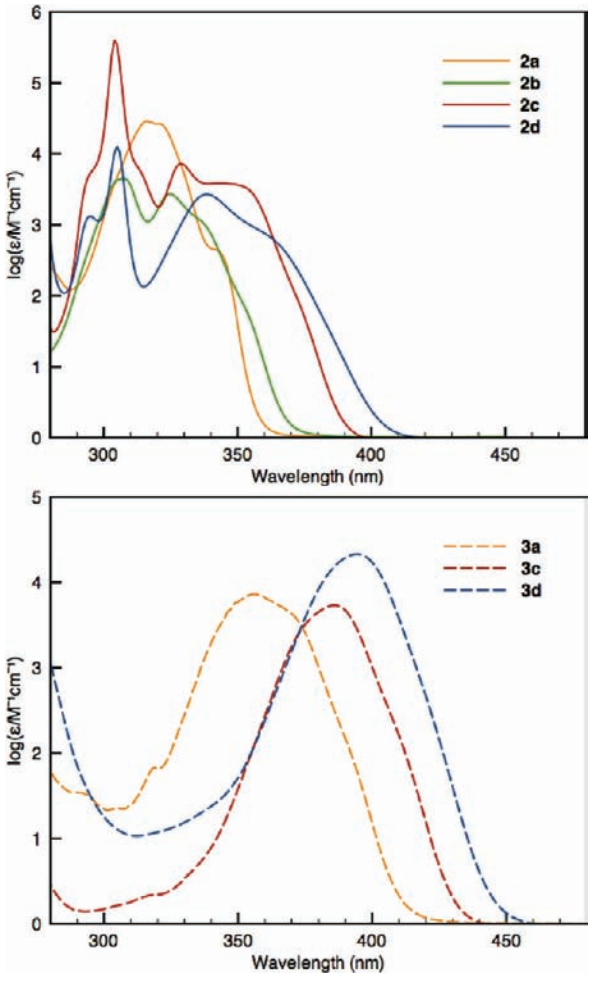

Figure 5. UV−vis absorption spectra of the sulfur(II) series **2** (top) and the sulfur dioxide series **3** (bottom) in CH_2Cl_2.

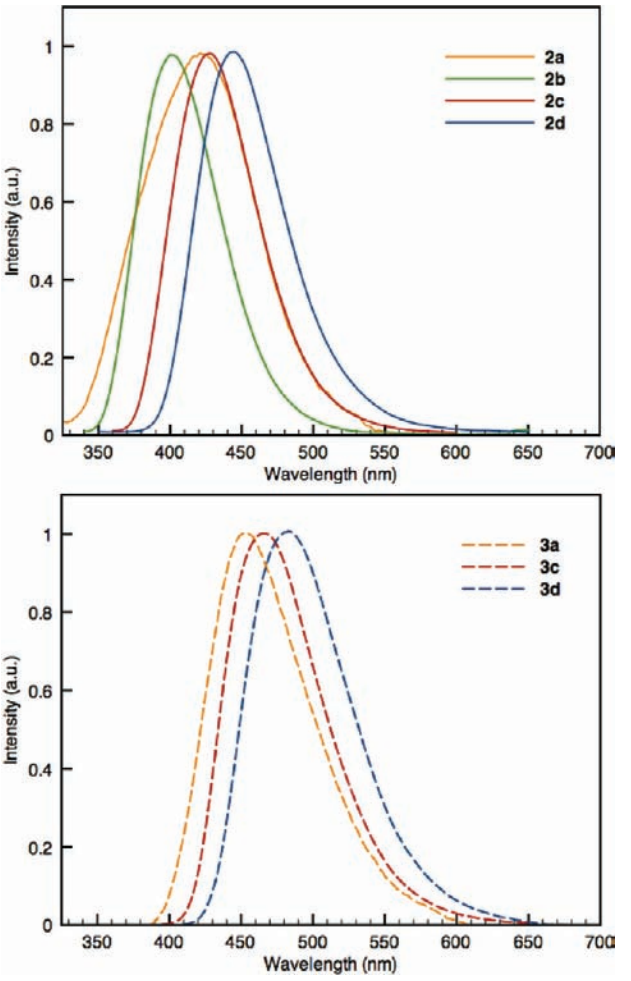

Figure 6. Normalized emission of the heterotetracenes in CH_2Cl_2 (top: sulfur(II) series **2**; bottom: sulfur dioxide series **3**).

2c shows the strongest solvent dependent emission properties (λ_{em} = 417 nm in cyclohexane; 428 nm in CH_2Cl_2; 427 nm in MeCN, and 434 nm in EtOH), which is consistent with the formation of a dipole between the sulfur (donor) and the phosphorus oxide (acceptor) centers (vide infra). Remarkably, compared to the somewhat related trivalent 1,4-dihydro-1,4-thiaphosphinine (**V**, E^1 = S, E^2 = lp, Chart 1; λ_{em} = 476 nm in CH_2Cl_2 and 446 nm in EtOH),[13b] trivalent phosphole **2a** does not show significant solvatochromism in either absorption (λ_{abs} = 319 nm in cyclohexane, 317 nm in CH_2Cl_2, 314 nm in EtOH, and 314 nm in CH_3CN) or emission (λ_{em} = 416 nm in cyclohexane, 421 nm in CH_2Cl_2, 421 nm in EtOH, and 425 nm in CH_3CN), probably due to a stronger delocalization of the phosphorus lone pair within the system (see theoretical section). The sulfur dioxide compounds **3a** and **3d** show stronger solvatochromism in their fluorescence emission relative to the non-oxidized sulfur(II) species **2a,d** (see Supporting Information). The comparatively stronger solvatochromism in the emission of **3a** and **3d** (relative to the absorption) indicates that oxidation of sulfur induces a more polarized structure in the excited state than in the ground state.[16] It needs to be mentioned, however, that **3d** is not stable in EtOH, which is probably due to the weakening of the phosphonium center and central C═C bond by the oxidation of sulfur allowing the EtOH to nucleophilically attack the phosphorus center.[10c,17]

Chart 2. Conjugation-Path Change upon Modification of the Phosphorus and Oxidation of the Sulfur Center

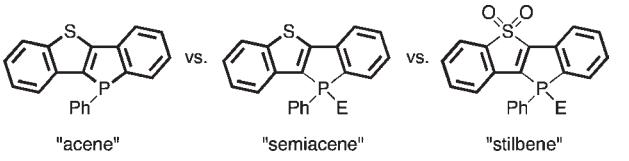

In the series **2a**−**d** and **3a**−**d**, the phosphorus oxide and phosphonium species (**2c**: ϕ_{PL} = 0.71; **2d**: ϕ_{PL} = 0.36, **3c**: ϕ_{PL} = 0.98, and **3d**: ϕ_{PL} = 0.99) generally show higher photoluminescence quantum yields than their congeners. Most of the compounds show lifetimes between τ = 10−15 ns, except for **2a** and **2b** that have lifetimes τ = 3.6 ns and τ = 2.6 ns, respectively. It should be noted that compounds **2a**, **3a**, and **3d** show biexponential-decay profiles (see Supporting Information) that were confirmed through excitation at varying wavelengths. Likely causes for this feature could be intramolecular charge transfer processes involving the exocyclic P-phenyl substituent and the main scaffold, or conformational changes involving the P-center and/or its phenyl substituent; in either case one lifetime component was clearly dominant (Table 2). The quantum yields and lifetimes allowed for the determination of relaxation processes from the

Table 2. Electrochemical Data for the Heterotetracenes

Compd	E_{red} [V][a] ($E_{pc1/pc2}$)	E_{ox} [V][a] (E_{pa})	EA [eV][b]	LUMO [eV][c]	HOMO [eV][c]
2a	–	0.88	–	−1.35	−5.53
2b	−1.45	–	–	−1.77	−5.90
2c[d]	−1.56[f] (−1.60/−1.52)	–	−3.04	−1.74	−5.80
2d[d,e]	−1.35	–	–	−2.64	−6.64
3a[d]	−1.84[f] (−2.01/−1.67)	0.64	−2.76	−2.11	−6.07
3c	−1.44[f] (−1.58/−1.29)	–	−3.16	−2.97	−6.65
3d[d,e]	−1.11, −1.53	–	–	−3.51	−7.11
4a	−2.07[f] (−2.20/−1.93)	–	−2.53	−2.34	−6.15
4b	−2.14[f] (−2.29/−1.99)	–	−2.46	−2.22	−6.13
5a	−1.78[f] (−1.89/−1.68)	–	−2.82	−2.91	−6.57

[a] Measured in CH_2Cl_2, with a Pt rod as working electrode, Pt wire as counter electrode, and Ag/AgCl/KCl 3 M as reference electrode; supporting electrolyte was NBu_4PF_6; Standard scan rate was 50 mV s^{-1}, $E_{red}(E_{ox}) = {}^1/_2(E_{pc} + E_{pa})$ for reversible or quasi-reversible process, otherwise $E_{red}(E_{ox}) = (E_{pa})$. [b] Electron affinities were calculated according ref 20. [c] Calculated at the B3LYP-6/31G(d)-level of theory. [d] X-ray crystallographic data were used as input files (counteranions were not included). [e] Polarizable continuum model (PCM, solvent = dichloromethane) was used. [f] Reversible or quasi-reversible redox process.

excited state (Figure 7). Since the fluorescence emission spectra that are governed by the main scaffold do not show any discernible fine structure that would result from competing processes, the average lifetimes were used for the calculation of the relaxation processes of **2a**, **3a**, and **3d**.[16] In **2a**, the large nonradiative rate constant $K_{nr} = 21.3 \times 10^{-7}\ s^{-1}$ is the major contributor to the low quantum yield. P-complexation with borane increases the radiative rate constant in **2b**, thus increasing the quantum yield. The both oxidation and methylation of the phosphorus center decrease the nonradiative rate constants significantly (**2c**: $K_{nr} = 3.6 \times 10^{-7}\ s^{-1}$, **2d**: $4.3 \times 10^{-7}\ s^{-1}$), which are likely the major cause for the higher quantum yield in the series **2a**−**d**. As for the sulfur dioxide series **3a**−**d**, the higher quantum yields of **3c** and **3d** are mainly due to both larger radiative constants (**3c**: $K_r = 7.6 \times 10^{-7}\ s^{-1}$, **3d**: $7.8 \times 10^{-7}\ s^{-1}$) and smaller nonradiative constants (**3c**: $K_{nr} = 0.2 \times 10^{-7}\ s^{-1}$, **3d**: $0.1 \times 10^{-7}\ s^{-1}$). An interesting trend is that, starting from **2a** ($\phi_{PL} = 0.24$) with sulfur(II) and phosphorus(III) centers, the fluorescence quantum yield increases more than three times when the phosphorus center is oxidized (**2c**: $\phi_{PL} = 0.71$), while the quantum yield actually decreases upon oxidation of the sulfur center (**3a**: $\phi_{PL} = 0.14$). Subsequent oxidation of the phosphorus center in **3c**, in turn, increases the quantum yield again ($\phi_{PL} = 0.98$). The larger extent of π-conjugation (A_π) of **2c** ($A_\pi = 5.48$), **3c** ($A_\pi = 8.24$), and **3d** ($A_\pi = 8.96$) relative to the others ($A_\pi = 3.44$ for **2a**, 4.11 for **2b**, 4.02 for **2d**, 2.75 for **3c**) also indicates that a positive phosphorus center (i.e., phosphorus oxide or phosphonium) increases the conjugation in the S_1 state of the heterotetracenes and provides a higher quantum yield (see theoretical section).[18]

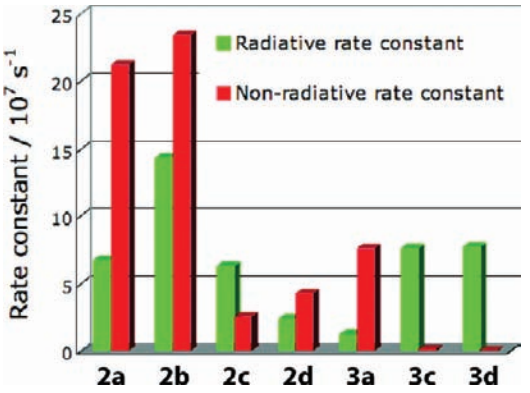

Figure 7. Rate constants of the tetracene series **2** and **3** in CH_2Cl_2.

2.4. Electrochemistry. The redox properties of the heterotetracenes can also provide valuable information on how the functionalized phosphorus and sulfur centers change the electronic properties of the system as a whole.[13b] The electrochemical properties of compounds **2a**−**d** and **3a**,**b**,**d** are summarized in Table 2 (see Supporting Information for CV spectra). Compared to BTBT that shows a reversible oxidation at $E_{ox} = +0.89$ V (vs Fc/Fc^+),[14a] **2a** shows an irreversible oxidation $E_{ox} = +0.88$ V (vs Fc/Fc^+) supporting a certain degree of delocalization of the phosphorus electron lone pair. By contrast, borane adduct **2b** only shows an irreversible reduction at $E_{red} = -1.45$ V, due to decreasing charge density at the phosphorus center that switches the redox properties of heteroacene core. Phosphole oxide **2c** exhibits a reversible reduction potential at $E_{red} = -1.56$ V, which is in line with other phosphole oxides reported by us earlier.[11f] The methylation affords a more positive phosphorus center, resulting in an irreversible reduction at $E_{red} = -1.35$ V that is also consistent with the lower LUMO energy of **2d** obtained from the theoretical calculations (vide infra). As provided by the photophysical studies, the system is switched to a diheteroatom-bridged stilbene system upon oxidation of the sulfur center. Sulfur dioxide **3a** shows a quasi-reversible reduction potential at $E_{red} = -1.84$ V and an irreversible oxidation at $E_{red} = +0.64$ V. The reduction process of **3a** could be rationalized by the electron-accepting character of the sulfur dioxide center, which is consistent with the more positive sulfur center (vide infra). The oxidation of phosphorus further enhances the electron-accepting character of the system, which is evident in a quasi-reversible reduction at $E_{red} = -1.44$ V for **3c**. As for **3d**, two reduction processes were observed, one at $E_{red} = -1.11$ V and another at $E_{red} = -1.53$ V. Compared to **3c**, the first more positive reduction of **3d** indicates that the methylation of phosphorus further enhances the electron-accepting character of the system as a whole.

The redox potential (next to thin film morphologies[19]) furthermore provides an indication on the potential charge injection character of the new materials that is important for practical device applications. Since all of the P-oxidized phosphole derivatives show reversible or quasi-reversible reduction, the solid-state electron affinity (EA) of the compounds was estimated from the electrochemically obtained electron injection (Table 2).[20] **3c** shows the highest EA value (ca. −3.2 eV) approaching that of the

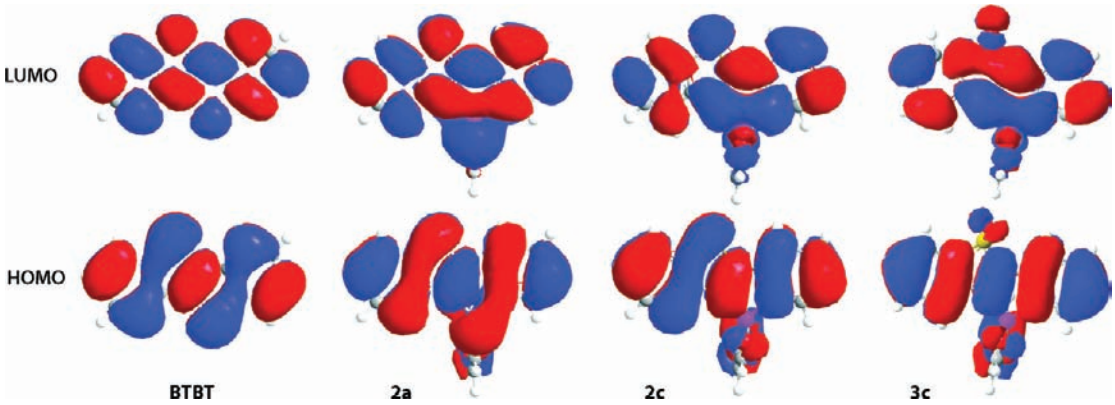

Figure 8. Frontier orbitals of BTBT, **2a**, **2c**, and **3c** (B3LYP/6-31G(d) level of theory).

well-established electron-transport material C_{60} (ca. −3.7 eV).[21] Furthermore, **2c** and **3c** show higher EA values (E_{EA} = ca. −2.8 eV for **2c**, ca. −3.0 eV for **3c**) than that of Alq_3 (−2.3 eV)[21] that is widely used as an electron-transport material in organic light-emitting diodes.

2.5. Theoretical Calculations. Theoretical calculations were carried out at the B3LYP/6-31G(d) level of theory[22] to reveal further details on the electronic nature of the new heterotetracenes; the energies of the HOMO and LUMO levels are summarized in Table 2. As reported previously, the frontier orbital energy levels can efficiently be modified by functionalization of the phosphorus center. Unlike in the dithienophosphole system,[10,11f] an interaction between the phosphorus lone pair and the π-system can be observed in the HOMO of **2a** (Figure 8). A similar interaction between sulfur and the π-system that is also observed in BTBT (**III**, $E^1 = E^2$ = S, Chart 1) supports the high degree of delocalization within the ring and could explain the similar absorption spectra of BTBT and **2a**.

However, the symmetry of the HOMO and LUMO orbitals of the phosphole analogues are distorted upon functionalization of the phosphorus center (BH_3, O, and Me^+), which is very likely the reason for the different absorption features of **2b**, **2c**, and **2d** relative to **2a**. Oxidation of sulfur converts this center into an electron acceptor, which in turn reestablishes the symmetry of the HOMO and LUMO orbitals in the sulfur dioxide series **3** (Figure 8; full details in the Supporting Information). Although the HOMO of **3a** also shows an interaction between the lone pair of phosphorus and the π-system, absorption and emission features support a more stilbene-like structure that is also consistent with the molecular structure of **3a** in the solid state. Moreover, the rigidified stilbene architecture enhances conjugation and narrows the band gap of the system. TD-DFT calculations were carried out in order to elucidate the transitions observed in the UV−vis spectra (see Supporting Information). All of the compounds were optimized at the B3LYP/6-31G(d) level theory and, where applicable, using the X-ray data as input files (**2c**, **2d**,[23] **3c**, and **3d**;[23] see Supporting Information). The trend in the calculated $S_0 \rightarrow S_1$ transition correlates well with the optical band gaps (see Supporting Information), except for **3a**, which is probably due to different conformations involving the pyramidalization of the phosphorus center and/or the exocyclic phenyl ring that exist in solution.[13b] As a consequence of the distorted orbital symmetry in the sulfur(II) series **2**, the $S_0 \rightarrow S_1$ transition of **2a** only originates from HOMO → LUMO, while the $S_0 \rightarrow S_1$ transitions of **2b**, **2c**, and **2d** also involve other energy levels (for details, see Supporting Information), highlighting the impact from the distorted symmetry of the molecular orbitals.

Other important information that could be obtained from the theoretical calculations relates to the charge distribution within the various derivatives. As expected, the phosphorus center becomes more positive through increasing its valency and concomitantly its coordination number (Table 3). The oxidation of sulfur decreases the electron density at this center significantly; as observed in the optical and the calculated band gaps, the more positive the sulfur center, the smaller the band gap of the P,S tetracenes. Surprisingly, in contrast to the nonoxidized sulfur(II) system, **3c** actually exhibits a higher electron density at phosphorus when compared to that of **3d**. These differences could be rationalized in terms of the oxidation of sulfur enhancing the communication between the sulfur and phosphorus centers due to the resulting relatively stronger electron acceptor character, i.e., S(VI) vs P(V), creating an inverted push−pull system. These features transform the oxidized phosphorus center into a donor, while the sulfur center remains the acceptor component. To counterbalance the electronic deficit at phosphorus, therefore, the generally very polar nature of the PO double bond (i.e., $P^+—O^-$) is reduced leading to a less polar form (i.e., P═O) with increased electron density at P, which is consistent with the NMR spectroscopy (vide supra). On the other hand, the spread between the Mulliken charges at the sulfur and phosphorus atoms is increased by the oxidation of sulfur, which is consistent with the solvatochromism in the emission of these compounds. In addition to the `rigidifying' effect of functionalized phosphorus, the electronic nature of phosphorus shows a similar trend as the fluorescence quantum yield; i.e., a more positive phosphorus center affords a higher quantum yield (Figure 9).

2.6. Functionalization of the Core. The high EA values of the heteroacene cores encouraged us to further improve the materials' properties, such as solubility, solid state organization, and film morphologies, which also play important roles in the fabrication and properties of organic electronics.[19] Alkylcarbonyl and perfluorophenylcarbonyl substituted oligothiophenes have been shown before to not only exhibit high charge carrier mobilities (p-type and n-type) but also facilitate solution-based device fabrication, which is very desirable with a view to low-cost processing.[24] Therefore, we were interested if the new heterotetracences could also be functionalized in a similar way and how the functionalization would influence the electronic and self-organization features of the core. Corresponding Friedel−Crafts acylation reactions were carried out between **2c** and suitable acyl chlorides (Scheme 4).

Table 3. Mulliken Charge Distributions; B3LYP-6/31G(d) Level of Theory

Compound	Mulliken charge of sulfur	Mulliken charge of phosphorus (sulfur)	Mulliken charge of oxygen	$\Delta\lvert P - S\rvert^a$
BTBT	0.234	0.234	NA	0
2a	0.224	0.409	NA	0.185
2b	0.242	0.572	NA	0.330
2c[b]	0.236	0.820	−0.545 (O=P)	0.584
2d[b,c]	0.314	0.669	NA	0.325
3a[b]	1.133	0.399	−0.488 (O=S)	0.734
			−0.502 (O=S)	
3c	1.867	0.417	−0.352 (O=S)	1.45
			−0.371 (O=S)	
			−0.474 (O=P)	
3d[b,c]	1.160	0.698	−0.462 (O=S)	0.484
			−0.465 (O=S)	

[a] Dipole strength calculated from the difference between Mulliken charge of sulfur and phosphorus. [b] X-ray crystallographic data were used as input files (counteranions were not included). [c] Polarizable continuum model (PCM, solvent = dichloromethane) was used.

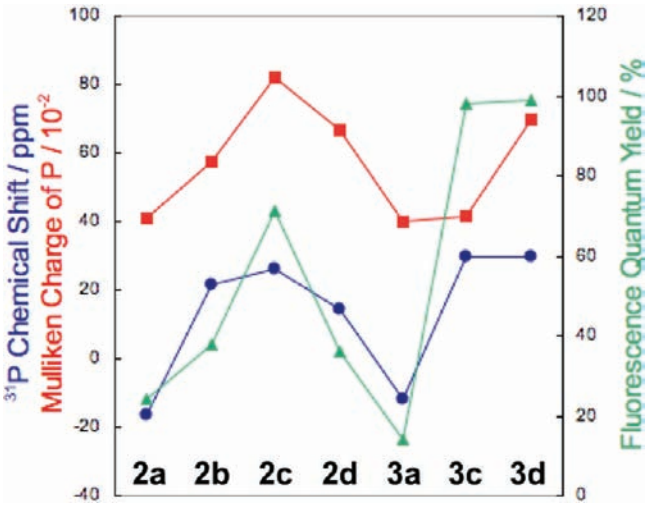

Figure 9. Trends between fluorescence quantum yield and the electronic nature of phosphorus; red: DFT calculated Mulliken charge of P/10^{-2}; blue: ^{31}P NMR shift ($CDCl_3$ at 298 K)/ppm; green: fluorescence quantum yield/%.

Surprisingly, the reaction between **2c** and hexanoyl chloride (even when applied in 3-fold excess) only resulted in the monosubstituted isomers **4a**/**4b** as the major products in a ratio of 2:3 that could be isolated through column chromatography. This reactivity is likely due to the electron-withdrawing effect of the oxidized phosphorus center, which decreases the reactivity of the benzene ring adjacent to the phosphole unit. The thienobenzene, on the other hand, is more electron-rich and thus activated for an electrophilic attack. The reaction between **2c** and 2 equiv of perfluorobenzoyl chloride also gave monosubstituted **5** as the only major product and further supported the deactivating effect of phosphorus oxide; in either case, only the thienobenzene ring can be acylated. Remarkably, monofunctionalization through Friedel−Crafts acylation is also observed with the somewhat

Scheme 4. Functionalization of the Core of 2c via Friedel−Crafts Acylation

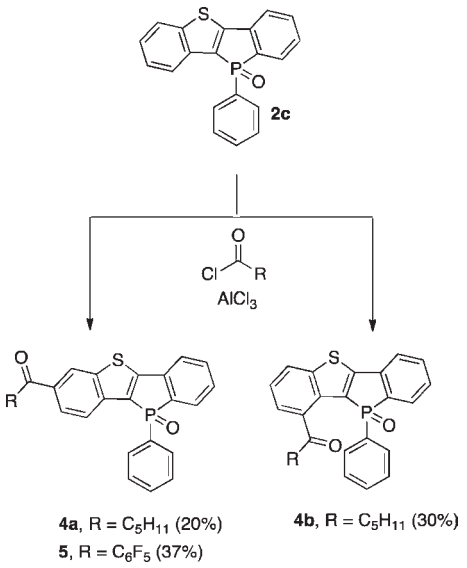

related dithienophosphole system.[25] As expected, the carbonyl group influences the photophysical properties in the extended heterotetracenes (Table 1). The lowest energy absorption maxima of the carbonyl compounds (**4a**: λ_{max} = 359 nm, **4b**: λ_{max} = 359 nm, **5**: λ_{max} = 368 nm) are red-shifted with respect to those of **2c** (Figure 10), which is consistent with the decreased HOMO−LUMO gaps from the theoretical calculations (ΔE = 3.81 eV for **4a**, 3.91 eV for **4b**, 3.66 eV for **5**). Notably, in the "*ortho*" isomer **4b**, the higher energy transition (at λ_{max} = 290−320 nm) is blue-shifted compared to that of **2c** and shows a smaller molar absorptivity than the low energy transition, while the opposite is true for the "*para*" isomer **4a**.

Although it is still not exactly clear what causes the spectral splitting at this stage, it is inherently plausible that the different locations of the acyl substituents are the reason for the altered electronic structures in **4a**/**4b**. On the other hand, the emission features of all three acylated compounds (λ_{em} = 427/428 nm) are similar to those of **2b**, and their low photoluminescence quantum yields (ϕ_{PL} = 0.13−0.29) are likely due to the quenching effect of the carbonyl moieties that has also been observed for aldehyde and ketone functionalized dithienophospholes.[25,26] Similar to the other phosphole oxides in the series **2a**−**d** and **3a**−**d**, all carbonyl-substituted derivatives exhibit one quasireversible reduction process (see Supporting Information for CV spectra). Compound **5** shows the most positive reduction at E_{red} = −1.78 V (vs Fc/Fc^+) due to the electron-poor perfluorophenyl group; the hexanoyl isomers show reduction potentials at E_{red} = −2.07 V for **4a** and −2.14 for **4b** (vs Fc/Fc^+). EA values of the extended cores (E_{EA} = −2.53 eV for **4a**, −2.46 eV for **4b**, −2.82 eV for **5**) are again higher than that of Alq_3 (−2.3 eV), albeit lower than the nonextended tetracenes (vide supra).

We were able to obtain suitable single crystals for X-ray crystallography of the acyl-extended compounds **4a**/**4b** and **5** from dichloromethane. Unfortunately, the structural parameters of **4b** were not good enough for a satisfying quantitative analysis of its molecular structure; however, the qualitative structural information still supported the position of the acyl substituent. To confirm the connectivity in **4b**, 2D NMR spectroscopy was carried out that further confirmed the position of the acyl

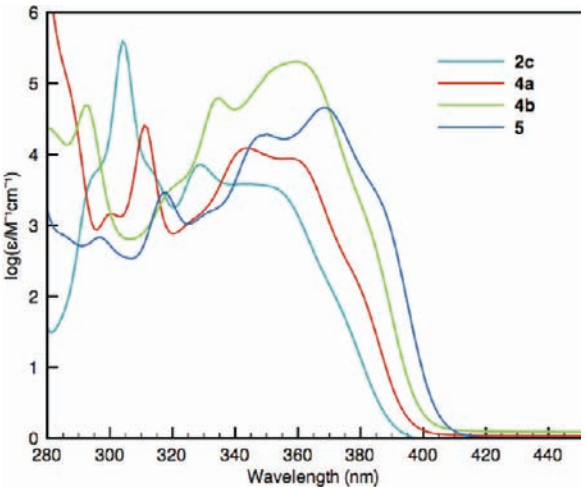

Figure 10. Absorption spectra of the extended acylated heterotetracenes vs **2c**.

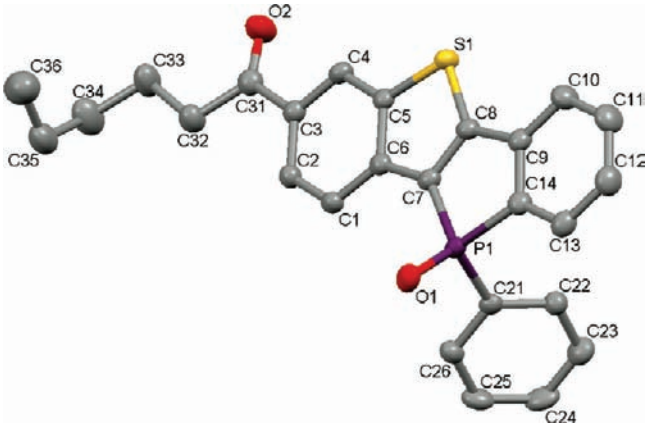

Figure 11. Molecular structure of **4a** in the solid state (50% probability level); hydrogen atoms are omitted for clarity. Selected bond lengths [Å] and angles [deg]: P1−O1: 1.478(18); P1−C7: 1.796(2); P1−C14: 1.807(3); P1−C21: 1.798(2); C7−C8: 1.364(3); C5−C6: 1.419(3); C9−C14: 1.400(3); S1−C5: 1.753(2); S1−C8: 1.723(2); C7−P1−C14: 92.02(12); C7−P1−C21: 109.12(11); C14−P1−C21: 107.61(11); C5−S1−C8: 90.27(12).

substituent (see Supporting Information). The structural data for **4a** and **5**, on the other hand, were acceptable for quantitatively determining their molecular structure in the solid state (Figures 11 and 12).

The carbonyl group does not change the structure of heterotetracene core very much. In **4a**, P−C (P1−C7: 1.796, P1−C14: 1.807, and P1−C21: 1.798 Å) and S−C (S1−C5: 1.753 and S1−C8: 1.723 Å) bonds are similar to those of **2c**. However, the pentafluorophenyl group in **5** is perpendicular (at 86.6°) to the tetracene core, which explains the small absorption red shift of this derivative relative to **2c**. Due to the perpendicular pentafluorophenyl arrangement suppressing potential extended intermolecular π-stacking interactions, **5** only associates into dimers in the solid state ($\pi-\pi$ distance: 3.6 Å; see Supporting Information).

Interestingly, the position of the hexanoyl group also has a significant effect on the macroscopic self-organization of **4a** and **4b** in the solid state. When attempting to grow crystals for X-ray crystallography, compound **4a** with the hexanoyl group along the

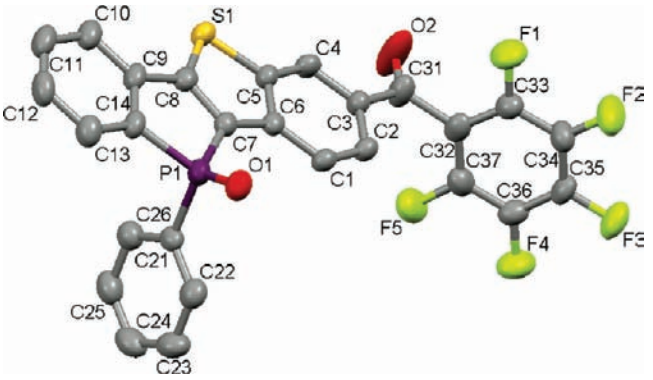

Figure 12. Molecular structure of **5** in the solid state (50% probability level); hydrogen atoms are omitted for clarity. Selected bond lengths [Å] and angles [deg]: P1−O1: 1.478(3); P1−C7: 1.797(5); P1−C14: 1.828(5); P1−C21: 1.809(5); C7−C8: 1.368(6); C5−C6: 1.411(6); C9−C14: 1.392(7); S1−C5: 1.753(4); S1−C8: 1.720(5); C7−P1−C14: 91.5(2); C7−P1−C21: 106.7(2); C14−P1−C21: 106.4(2); C5−S1−C8: 90.4(2).

long axis of the main tetracene scaffold precipitated from the solvent mixture (acetone/hexane: 4/1) in the shape of fibers upon slow evaporation at room temperature. Using optical and fluorescence microscopy, microfibers with lengths of ca. 30−40 μm and widths of up to 5 μm could indeed be observed (Figure 13a and b). Scanning Electron Microscopy (SEM) of the precipitated **4a** (Figure 13c and d) further confirmed the formation of 1D microfibers in the solid state, but also that they consist of bundles of smaller fibers. The red-shifted solid-state absorption of the microfibers compared with that of **4a** in CH_2Cl_2 solution (Figure 14) suggests that $\pi-\pi$ interactions play a role in the 1D self-assembly process. Such 1D organic nano-/micromaterials have recently attracted significant attention, due to their efficient energy transfer and charge carrier transport features, as well as high ionic conductivity.[27] By contrast, the "*ortho*" hexanoyl isomer **4b** does not show a similar self-organization process into 1D microfibers. Under the same conditions (acetone/hexane: 4/1), **4b** only precipitates as a crystalline powder, as verified via SEM (Figure 13e and f).

Exposing the nonextended heterotetracene cores (**2a**−**d** and **3a**,**b**,**d**) to similar conditions (acetone/hexane: 4/1; room temperature) did not afford the analogous precipitation of 1D microfibers. Instead, amorphous powders or polycrystalline solids were obtained only upon complete evaporation of the solvents. To further investigate the self-organization process, **4a** and **4b** were also exposed to a variety of different solvents (neat acetone, dichloromethane, ethyl acetate, and THF), which also did not result in the precipitation of similar 1D microfibers during evaporation at room temperature, but a similar behavior as that for the nonextended core systems (amorphous powders/polycrystalline solids only after complete evaporation of the solvents).

Notably, the ^{1}H NMR spectrum of the dissolved fibers of **4a** reveals that acetone is part of the fibers, as a corresponding signal at 2.17 pm can be observed that integrates to a ratio of 3:1 (**4a**/acetone). To further support the presence of acetone, the X-ray diffraction (XRD) pattern of the **4a** microfibers shows distinctly different structural features from the bulk crystals of **4a** (see Supporting Information). By contrast, the XRD of the crystalline sample of **4b** (from acetone/hexane: 4/1) shows an almost identical structure pattern to that of the bulk crystals (see Supporting Information). To gain some deeper insight into the interaction

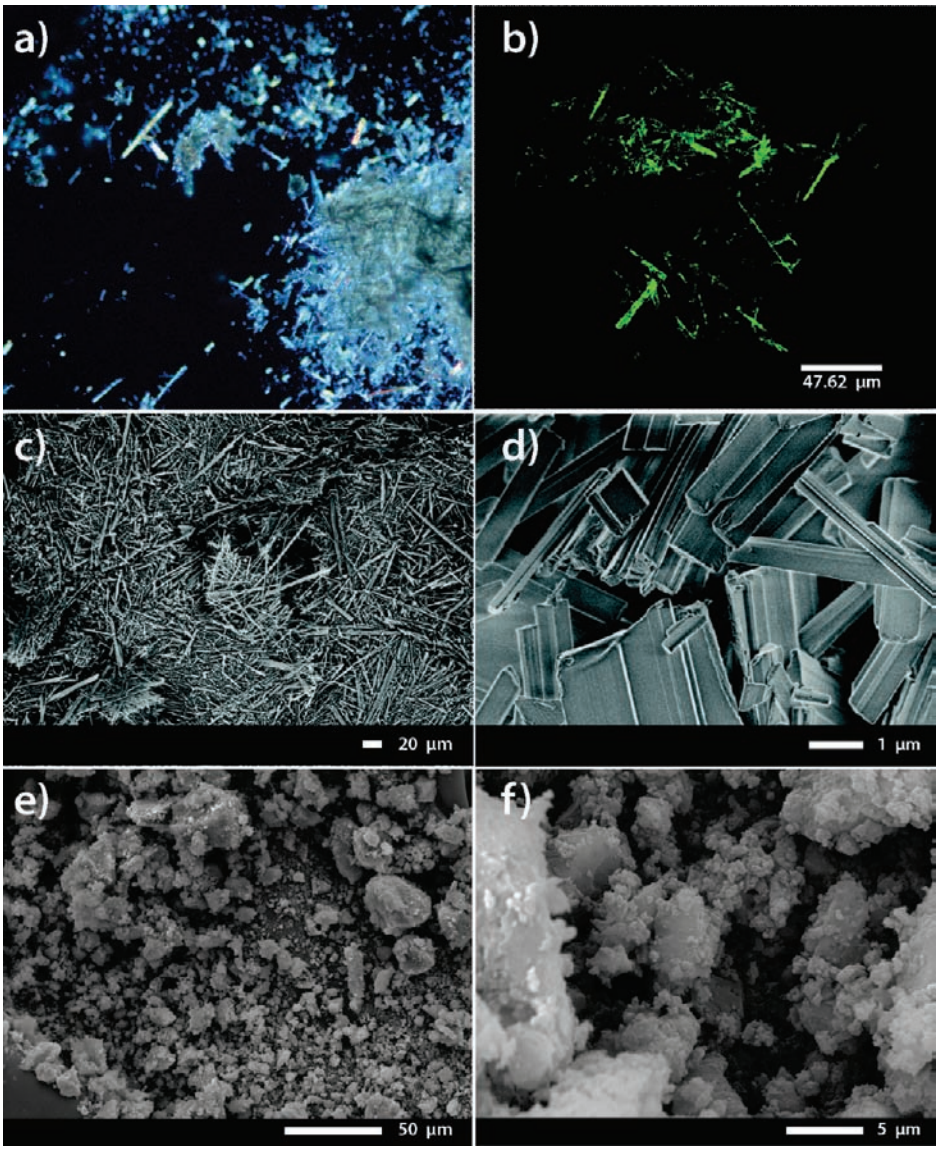

Figure 13. Images of the microstructures of **4a** ((a) polarized optical microscopy; (b) fluorescence confocal miscroscopy; (c and d) SEM at different scales) and **4b** ((e and f) SEM at different scales).

between **4a** and acetone in the microfibers, we have performed additional IR and ^{13}C NMR spectroscopy experiments, but potential electrostatic or hydrogen-bonding interactions could not be detected. In turn however, slow evaporation of acetone from the fibers could be detected by ^{1}H NMR, showing only about 12% of residual acetone after about a month. The latter suggests that acetone may simply be trapped in the voids of the solid-state organization between the molecules of **4b** without any directed polar interactions. This feature could also be supported by Differential Scanning Calorimetry (DSC) of the microfibers of **4a**. DSC also confirmed the presence of acetone, showing not only a sharp melting transition at T_m = 169.0 °C (see Supporting Information) but also a broad endothermal transition around 87 °C (the evaporation of acetone) in the first heating scan; thermogravimetric analysis (TGA) corroborates the loss of acetone at 67.2 °C. In the second heating scan, only a broad glass transition at T_g = 46.2 °C can be observed, which is similar to the DSC results for the nonfunctionalized cores (**2b,c,d** and **3a,c,d**) showing a sharp melting transition in the first heating scan and a broad glass transition in the second heating scan (see Supporting Information). The "*ortho*" isomer **4b**, on the other hand, shows a significantly different thermal transition behavior. In the first and second heating scan, a sharp endothermic transition (melting) could be observed at T_m = 195.8 °C. But unlike **4a**, the first cooling process results in a sharp shape exothermic transition (T_c = 140.5 °C) indicating the crystallization of **4b** (see Supporting Information).

Based on these initial studies, the exclusive formation of 1D microfibers from **4a** can be rationalized by three common factors generally employed for self-organizing acenes:[27,28] (1) the polar moieties (P═O and C═O) and solubilizing group (alkyl chain) in heterotetracenes could direct molecules to self-assemble along a certain direction through intermolecular interactions (dipole−dipole interaction, $\pi-\pi$ stacking, and H/π edge-to-face interactions). Similar dipole−dipole effects have been found in dialkoxyl substituted acene systems; (2) the correct solvent mixture containing "good" (acetone) and "bad" (hexane) solvents helping the formation of 1D microfibers through solution-based self-organization processes; and (3) the appropriate linear rod−coil structure of

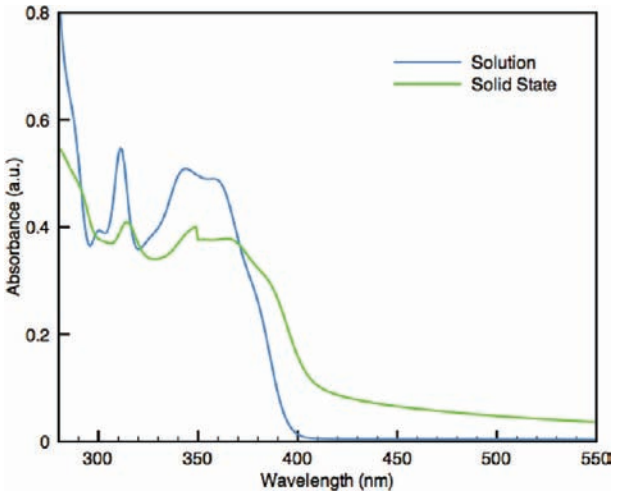

Figure 14. Absorption of the fibers of **4a**, as solid and dissolved in CH_2Cl_2.

4a (as opposed to the "nondirectional", skewed molecular structure of **4b**) for different favorable 1D-directional intermolecular interactions. In order to generate further well-defined micro-/nanostructures from this new heterotetracene system, detailed investigations on the specific molecular design (degree of conjugation, alkyl chain length), solvent effects (polarity and concentration), and temperature effect during the self-organization processes are now being carried out in our laboratory.

3. CONCLUSIONS

In summary, we have synthesized a new phosphorus-based heterotetracene core as a new member of the oligoacene family and have extended the system through acylation. This structure—property study further revealed the effect of incorporation of phosphorus centers into ladder-type π-conjugated systems. For the first time, we could demonstrate that sulfur as the secondary heteroatom can also be oxidized readily. The different electronic natures of the heteroatoms allowed independent functionalization of the phosphorus and sulfur centers, respectively. Although the oxidation of the sulfur center is not reversible under the employed conditions, the phosphorus center can reversibly be modified in both directions (oxidation *and* reduction). Therefore, the reactivity of the latter *de facto* provides for full control over the oxidation states of both heteroatom centers. UV—vis spectroscopy and fluorescence studies showed that the oxidation of sulfur not only influences the electronic contribution of phosphorus but also alters the general conjugation pathway of the heterotetracene system (from benzothienobenzophosphole to stilbene), which is supported by ^{31}P NMR spectroscopy and X-ray crystallography, as well as theoretical calculations. More importantly, the theoretical studies allowed us to correlate the photophysical properties with the different electronic natures of sulfur and phosphorus. In this dually switchable system, the band gap of the system is mainly controlled by the electronic nature of sulfur, while the photoluminescence quantum yield highly depends on the electronic nature of phosphorus. Cyclic voltammetry revealed that the redox properties of these S,P heterotetracenes can be altered by the electronic nature of heteroatoms. Particularly, the electron-accepting character and higher electron affinity of the oxidized S/P species make them promising candidates for n-type semiconducting materials. Furthermore, the functionalization of the phosphorus-based tetracene core with long alkyl chains provides access to intriguing 1D-microstructures and thus opens the door for phosphole chemistry to be used in self-assembling organic π-conjugated materials. Systematic studies toward corresponding phosphole-based systems are therefore currently underway in our group and will be reported in due course.

■ ASSOCIATED CONTENT

Supporting Information. Full experimental details for the synthesis of all new compounds. CIF files of all structures determined by X-ray crystallography and intermolecular packing interactions of all crystallographically characterized compounds. Solvatochromism data and TD-DFT data for compounds **2a**—**d**, **3a**,**c**,**d**. Frontier orbitals for compounds **2a**—**c**, **3a**,**b**,**d**, **4a**,**b**, and **5** (B3LYP/6-31G(d)-level of theory). Cyclic voltammograms for compounds **2a**—**d**, **3a**,**c**,**d**, **4a**,**b**, and **5**. Thermal (DSC and TGA) traces of compounds **4a**,**b** and **5**. SEM images of the microfibers of **4a**. XRD and IR spectra of **4a** and **4b**. Fluorescence lifetime measurements for compounds **2a**—**d** and **3a**,**c**,**d**. This material is available free of charge via the Internet at http://pubs.acs.org.

■ AUTHOR INFORMATION

Corresponding Author
Thomas.baumgartner@ucalgary.ca

■ ACKNOWLEDGMENT

Financial support by NSERC of Canada and the Canada Foundation for Innovation (CFI) is gratefully acknowledged. We also thank Alberta Ingenuity, now part of Alberta Innovates - Technology Futures for a graduate scholarship (Y.R.) and a New Faculty Award (T.B.). Thanks is given to Prof. C. P. Berlinguette for access to fluorescence instruments and Prof. T. Sutherland for his help with the electrochemical studies. The authors would also like to thank Dr. T. Gordon and P. G. Bomben for help with fluorescence quantum yield and lifetime experiments, Prof. S. Trudel for help with the SEM of **4a**, and Prof. V. Thangadurai as well as J. Kan for the access to powder X-ray diffraction.

■ REFERENCES

(1) (a) Scherf, U. *J. Mater. Chem.* **1999**, *9*, 1853. (b) Watson, M. D.; Fechtenkötter, A.; Müllen, K. *Chem. Rev.* **2001**, *101*, 1267. (c) Anthony, J. E. *Chem. Rev.* **2006**, *106*, 5028. (d) Anthony, J. E. *Angew. Chem., Int. Ed.* **2007**, *46*, 2.

(2) (a) Fukazawa, A.; Yamaguchi, S. *Chem.—Asian J.* **2009**, *15*, 1386. (b) Bosdet, M. J. D.; Piers, W. E. *Can. J. Chem.* **2009**, *87*, 8. (c) Baumgartner, T. *J. Inorg. Organomet. Polym. Mater.* **2005**, *15*, 389.

(3) Xiao, K.; Liu, Y.; Qi, T.; Zhang, W.; Wang, F.; Gao, J.; Qiu, W.; Ma, Y.; Cui, G.; Chen, S.; Zhan, X.; Yu, G.; Qin, J.; Hu, W.; Zhu, D. *J. Am. Chem. Soc.* **2005**, *127*, 13281. (b) Yamada, K.; Okamoto, T.; Kudoh, K.; Wakamiya, A.; Yamaguchi, S.; Takeya, J. *Appl. Phys. Lett.* **2007**, *90*, 072102.

(4) (a) Curtis, M. D.; Cao, J.; Kampf, J. W. *J. Am. Chem. Soc.* **2004**, *126*, 4318. (b) Kim, E.-G.; Coropceanu, V.; Gruhn, N. E.; Sánchez-Carrera, R. S.; Snoeberger, R.; Matzger, A. J.; Brédas, J.-L. *J. Am. Chem. Soc.* **2007**, *129*, 13072.

(5) (a) Amir, E.; Rozen, S. *Angew. Chem., Int. Ed.* **2005**, *44*, 7374. (b) Barbarella, G.; Favaretto, L.; Zambianchi, M.; Pudova, O.; Arbizzani, C.; Bongini, A.; Mastragostino, M. *Adv. Mater.* **1998**, *10*, 551. (c) Tedesco, E.; Sala, F. D.; Favaretto, L.; Barbarella, G.; Albesa-Jové, D.; Pisignano, D.; Gigli, G.; Cingolani, R.; Harris, K. D. M. *J. Am. Chem. Soc.* **2003**, *125*, 12277.

(6) (a) Suzuki, Y.; Okamoto, T.; Wakamiya, A.; Yamaguchi, S. *Org. Lett.* **2008**, *10*, 3393. (b) Shefer, N.; Harel, T.; Rozen, S. *J. Org. Chem.* **2009**, *74*, 6993. (c) Miguel, L. S.; Matzger, A. J. *J. Org. Chem.* **2008**, *73*, 7882.

(7) (a) Elbing, M.; Bazan, G. C. *Angew. Chem., Int. Ed.* **2008**, *47*, 834. (b) Mercier, L. G.; Piers, W. E.; Parvez, M. *Angew. Chem., Int. Ed.* **2009**, *48*, 6108. (c) Bosdet, M. J. D.; Piers, W. E.; Sorensen, T. S.; Parvez, M. *Angew. Chem., Int. Ed.* **2007**, *46*, 4940. (d) Jaska, C. A.; Piers, W. E.; McDonald, R.; Parvez, M. *J. Org. Chem.* **2007**, *72*, 5234. (e) Agou, T.; Kobayashi, J.; Kawashima, T. *Chem.—Eur. J.* **2007**, *13*, 125. (f) Agou, T.; Kobayashi, J.; Kawashima, T. *Chem. Commun.* **2007**, 3204. (g) Agou, T.; Kobayashi, J.; Kawashima, T. *Org. Lett.* **2006**, *8*, 2241.

(8) For silicon, see: (a) Yamaguchi, S.; Xu, C.; Tamao, K. *J. Am. Chem. Soc.* **2003**, *125*, 13662. (b) Xu, C.; Wakamiya, A.; Yamaguchi, S. *J. Am. Chem. Soc.* **2005**, *127*, 1638. (c) Mouri, K.; Wakamiya, A.; Yamada, H.; Kajiwara, T.; Yamaguchi, S. *Org. Lett.* **2007**, *9*, 93. (d) Biaso, F.; Geoffroy, M.; Canadell, E.; Auban-Senzier, P.; Levillain, E.; Fourmigué, M.; Avarvari, N. *Chem.—Eur. J.* **2007**, *13*, 5394. (e) Shimizu, M.; Tatsumi, H.; Mochida, K.; Oda, K.; Hiyama, T. *Chem.—Asian J.* **2008**, *3*, 1238.

(9) For phosphorus, see: (a) Matano, Y.; Imahori, H. *Org. Biomol. Chem.* **2009**, *7*, 1258; (b) Baumgartner, T; Réau, R. *Chem. Rev.* **2006**, *106*, 468; Correction: *Chem. Rev.* **2007**, *108*, 303. (c) Crassous, J.; Réau, R. *Dalton Trans.* **2008**, 6865. (d) Washington, M. P.; Gudimetla, V. B.; Laughlin, F. L.; Deligonul, N.; He, S.; Payton, J. L.; Simpson, M. C.; Protasiewicz, J. D. *J. Am. Chem. Soc.* **2010**, *132*, 4566. (e) Dillon, K. B.; Mathey, F.; Nixon, J. F. *Phosphorus: The Carbon Copy*; Wiley: New York, 1998. (f) Mathey, F. *Phosphorus-Carbon Heterocyclic Chemistry: The Rise of a New Domain*; Pergamon Press: Amsterdam, 2001.

(10) (a) Baumgartner, T.; Neumann, T.; Wirges, B. *Angew. Chem., Int. Ed.* **2004**, *43*, 6197. (b) Baumgartner, T.; Bergmans, W.; Kárpáti, T.; Neumann, T.; Nieger, M.; Nyulászi, L. *Chem.—Eur. J.* **2005**, *11*, 4687. (c) Durben, S.; Dienes, Y.; Baumgartner, T. *Org. Lett.* **2006**, *8*, 5893. (d) Dienes, Y.; Durben, S.; Kárpáti, T.; Neumann, T.; Englert, U.; Nyulászi, L.; Baumgartner, T. *Chem.—Eur. J.* **2007**, *13*, 7487. (e) Hobbs, M. G.; Baumgartner, T. *Eur. J. Inorg. Chem.* **2007**, 3611.

(11) (a) Fukazawa, A.; Hara, M.; Son, T.; Okamoto, E.-C.; Xu, C.; Tamao, K.; Yamaguchi, S. *Org. Lett.* **2008**, *10*, 913. (b) Fukazawa, A.; Ichihashi, Y.; Kosaka, Y.; Yamaguchi, S. *Chem.—Asian J.* **2009**, *4*, 1729. (c) Saito, A.; Miyajima, T.; Nakashima, M.; Fukushima, T.; Kaji, H.; Matano, Y.; Imahori, H. *Chem.—Eur. J.* **2009**, *15*, 10000. (d) Miyajima, T.; Matano, Y.; Imahori, H. *Eur. J. Org. Chem.* **2008**, 255. (e) Matano, Y.; Miyajima, T.; Fukushima, T.; Kaji, H.; Kimura, Y.; Imahori, H. *Chem.—Eur. J.* **2008**, *14*, 8102. (f) Dienes, Y.; Eggenstein, M.; Kárpáti, T.; Sutherland, T. C.; Nyulászi, L.; Baumgartner, T. *Chem.—Eur. J.* **2008**, *14*, 9878. (g) Ren, Y.; Dienes, Y.; Hettel, S.; Parvez, M.; Hoge, B.; Baumgartner, T. *Organometallics* **2009**, *28*, 734.

(12) (a) Fukazawa, A.; Yamada, H.; Sasaki, Y.; Akiyama, S.; Yamaguchi, S. *Chem.—Asian J.* **2010**, *5*, 466. (b) Fukazawa, A.; Yamada, H.; Yamaguchi, S. *Angew. Chem., Int. Ed.* **2008**, *47*, 5582.

(13) (a) Ren, Y.; Linder, T.; Baumgartner, T. *Can. J. Chem.* **2009**, *87*, 1222. (b) Ren, Y.; Baumgartner, T. *Chem.—Asian J.* **2010**, *5*, 1918.

(14) (a) Ebata, H.; Izawa, T.; Miyazaki, E.; Takimiya, K.; Ikeda, M.; Kuwabara, H.; Yui, T. *J. Am. Chem. Soc.* **2007**, *129*, 15732. (b) Izawa, T.; Miyazaki, E.; Takimiya, K. *Adv. Mater.* **2008**, *20*, 3388. (c) Sundar, V. C.; Zaumseil, J.; Podzorov, V.; Menard, E.; Willett, R. L.; Someya, T.; Gershenson, M. E.; Rogers, J. A. *Science* **2004**, *303*, 1644. (d) da Silva Filho, D. A.; Kim, E.-G.; Brédas, J.-L. *Adv. Mater.* **2005**, *17*, 1072.

(15) Aaron, J.-J.; Mechbal, Z.; Adenier, A.; Parkanyi, C.; Kozmik, V.; Svoboda, J. *J. Fluoresc.* **2002**, *12*, 231.

(16) (a) Lakowicz, J. R. *Principles of Fluorescence Spectroscopy*, 3rd ed.; Springer: New York, 2006. (b) Valeur, B. *Molecular Fluorescence, Principles and Applications*; Wiley-VCH: Weinheim, 2002.

(17) Nakayama, J.; Sugihara, Y. *Top. Curr. Chem.* **1999**, *205*, 132.

(18) Yamaguchi, Y.; Matsubara, Y.; Ochi, T.; Wakamiya, T.; Yoshida, Z. *J. Am. Chem. Soc.* **2008**, *130*, 13867.

(19) (a) Cicoira, F.; Santato, C.; Dinelli, F.; Murgia, M.; Loi, M. A.; Biscarini, F.; Zamboni, R.; Heremans, P.; Muccini, M. *Adv. Funct. Mater.* **2005**, *15*, 375. (b) Foerster, T. *Ann. Phys. (Leipzig)* **1984**, *2*, 55. (c) Pope, M. *Electronic Processes In Organic Crystals*; Clarendon Press: Oxford, 1982. (d) Kenkre, V. M.; Peineker, P. *Exciton Dynamics in Molecular Crystals and Aggregates*; Springer: Berlin, 1982. (e) Muccini, M.; Murgia, M.; Biscarini, F.; Taliani, C. *Adv. Mater.* **2001**, *13*, 355. (f) Duan, L.; Hou, L. D.; Lee, T.-W.; Qiao, J.; Zhang, D. Q.; Dong, G. F.; Wang, L. D.; Qiu, Y. *J. Mater. Chem.* **2010**, *20*, 6392.

(20) (a) Anderson, J. D.; et al. *J. Am. Chem. Soc.* **1998**, *120*, 9646. (b) Hreha, R. D.; George, C. P.; Haldi, A.; Domercq, B.; Malagoli, M.; Barlow, S.; Brédas, J.-L.; Kippelen, B.; Marder, S. R. *Adv. Funct. Mater.* **2003**, *13*, 967.

(21) Cahen, D.; Kahn, A. *Adv. Mater.* **2003**, *15*, 271.

(22) Frisch, M. J.; et al. *Gaussian 03*, revision E.01; Gaussian Inc.: Wallingford, CT, 2007 (see Supporting Information for full reference)

(23) Only the cationic part has been used for these compounds, as the materials' electronic properties are usually governed by the cation. To account for this truncation, a polarizable continuum model (PCM) with solvent = dichloromethane was used for the calculations.

(24) (a) Letizia, J. A.; Cronin, S.; Ortiz, R. P.; Facchetti, A.; Ratner, M. A.; Marks, T. J. *Chem.—Eur. J.* **2009**, *16*, 1911. (b) Chen, M. C.; Chiang, Y. J.; Kim, C.; Guo, Y. J.; Chen, S. Y.; Liang, Y. J.; Hu, T. S.; Lee, G. H.; Facchetti, A.; Marks, T. J. *Chem. Commun* **2009**, 1846.

(25) Gordon, T. J.; Szabo, L. D.; Linder, T.; Berlinguette, C. P.; Baumgartner, T. *C. R. Chimie* **2010**, *13*, 971.

(26) Romero-Nieto, C.; Merino, S.; Rodríguez-López, J.; Baumgartner, T. *Chem.—Eur. J.* **2009**, *15*, 4135.

(27) (a) Zhang, L.; Che, Y.; Moore, J. S. *Acc. Chem. Res.* **2008**, *41*, 1596. (b) Li, R. P.; Hu, W. P.; Liu, Y. Q.; Zhu, D. B. *Acc. Chem. Res.* **2008**, *41*, 529. (c) Zhao, Y. S.; Fu, H. B.; Peng, A. D; Ma, Y.; Liao, Q.; Yao, J. N. *Acc. Chem. Res.* **2010**, *43*, 509. (d) Kato, T. *Angew. Chem., Int. Ed.* **2010**, *49*, 2.

(28) (a) Olive, A. G. L.; Guerzo, A. D.; Belin, C.; Reichwagen, J.; Desvergne, J.-P. *Res. Chem. Intermed.* **2008**, *34*, 137. (b) Desvergne, J.-P.; Olive, A. G. L.; Sangeetha, N. M.; Reichwagen, J.; Hopf, H.; Guerzo, A. D. *Pure Appl. Chem.* **2006**, *78*, 2333. (c) Desvergne, J.-P.; Guerzo, A. D.; Bouas-Laurent, H.; Belin, C.; Reichwagen, J.; Hopf, H. *Pure Appl. Chem.* **2006**, *78*, 707. (d) Guerzo, A. D.; Olive, A. G. L.; Reichwagen, J.; Hopf, H.; Desvergne, J.-P. *J. Am. Chem. Soc.* **2005**, *127*, 17984. (e) Reichwagen, J.; Hopf, H.; Guerzo, A. D.; Belin, C.; Bauas-Laurent, H.; Desvergne, J.-P. *Org. Lett.* **2005**, *7*, 971.